



## Research Article

# The Preparation of Eco-Friendly Magnetic Adsorbent from Wild Water Hyacinth (*Eichhornia crassipes*): The Application for Removing Lead Ions from Industrial Wastewater

Thien Khanh Tran <sup>1</sup>, Quang Dung Le,<sup>2</sup> Thi Muoi Vo,<sup>3</sup> Minh Quang Diep,<sup>3</sup>  
Thanh Duy Nguyen,<sup>3</sup> Hau Huu Huynh,<sup>3</sup> Quoc Khanh Ly,<sup>3</sup> and Namkeun Kim <sup>4</sup>

<sup>1</sup>Chemical Engineering in Advanced Materials and Renewable Energy Research Group, School of Engineering and Technology, Van Lang University, Ho Chi Minh City, Vietnam

<sup>2</sup>The Institute for Circular Economy Development (ICED), Vietnam National University Ho Chi Minh City, Linh Trung, Thu Duc City, Ho Chi Minh City, Vietnam

<sup>3</sup>Faculty of Applied Sciences, Ton Duc Thang University, 19th Nguyen Huu Tho, Ward Tan Phong, District 7, Ho Chi Minh City 700000, Vietnam

<sup>4</sup>Department of Mechanical Engineering, Sogang University, Republic of Korea

Correspondence should be addressed to Thien Khanh Tran; [thienkhanhtran2211@gmail.com](mailto:thienkhanhtran2211@gmail.com) and Namkeun Kim; [nkim@sogang.ac.kr](mailto:nkim@sogang.ac.kr)

Received 15 April 2022; Revised 29 June 2022; Accepted 26 July 2022; Published 22 August 2022

Academic Editor: Muhammad Raziq Rahimi Kooch

Copyright © 2022 Thien Khanh Tran et al. This is an open access article distributed under the Creative Commons Attribution License, which permits unrestricted use, distribution, and reproduction in any medium, provided the original work is properly cited.

Water hyacinth (*Eichhornia crassipes*) is a wild floating plant that can be found widely in pond or river areas. The plant grows fiercely and causes many harmful issues to the ecosystem around its covered area. This work provides a utilization method that converts wild water hyacinth to reliable magnetic biochar which can be used as a very effective adsorbent for the removal of lead ion Pb(II) in industrial wastewater. The mentioned magnetic biochar can be prepared via a modified pyrolysis process at 550°C with the support of cobalt sulfates as magnetite precursors and limited oxygen from the sweeping gas (the gas mixture ratio is 4:1 nitrogen/oxygen). The produced samples were hydrophobic biochar with high oxygen-containing functional groups that are suitable for the removal of inorganic contaminants. The impregnation of cobalt (II, III) oxides provided high magnetic separation performance and additional adsorption sites on the produced magnetic biochar. As indicated by the obtained result, the WHB-Co2M sample possesses a highly porous structure (0.126 cc/g), higher thermal stability (thermal durability reaches 900°C), relatively stable magnetic properties (14.74 emu/g), and a larger surface area (192 m<sup>2</sup>/g). These beneficial properties led to its suitability to serve as an adsorbent in removing lead ions in the contaminated effluent, recording 95% of removal efficiency and adsorption capacity of 67.815 mg/g. As indicated in the result, all prepared magnetic biochar samples were fitted to two-parameter (Langmuir models) and three-parameter (Sips model) isotherm models. Therefore, the adsorption process in this work could be carried out on both homogeneous and heterogeneous adsorbent surfaces. The adsorption kinetics of the removal process also was described by the pseudo-first-order, pseudo-second-order, and Elovich models to reveal the adsorption and desorption rate of the as-prepared magnetic biochar. This work indicates a successful waste refinery route of converting lignocellulosic biomass such as water hyacinth into value-added material for use as promising heavy metal adsorbents.

## 1. Introduction

Nowadays, the intense industrialization and modernization in many countries around the world have led to several environmental problems, especially the heavy metals pollution in industrial wastewater. Contamination of heavy metals could be related to wastes from many industries, such as the plating industry, mining, tanneries, and the circuit board industry [1]. Lead, tin, and nickel are the most popular metals used in the manufacturing of circuit boards as resistant plates [2]. In particular, lead is the most commonly used material, despite its high toxicity and widespread presence in the environment [3]. Lead is also the main factor causing anemia, kidney malfunction, brain damage, and even death in some significant poisoning conditions [4]. These facts motivate the development of effective solutions to remove lead ions Pb(II) from contaminated sources. In that manner, this work proposed a method to eliminate Pb(II) in the printed circuit boards manufacturing wastewater, using adsorbents derived from water hyacinth (*Eichhornia crassipes*). Water hyacinth is an aquatic plant typically found in lakes and other basins, causing numerous conservation problems. The growth of the plant is very aggressive, and its ability to spread over the surface of body water was reported to lead to the degradation of water quality by altering the physical, chemical, and biological processes in the covered areas [5]. The floating plants form dense and thick brush over the water surface, providing a breeding ground for mosquitoes, restricting access to water, damaging the natural wetlands, and also eliminating other aquatic plants [6].

Generally, the water hyacinth is utilized as livestock feed; however, the effectiveness of this utilization plan has been reduced over time due to the popularization of formulated feeds. Therefore, turning overgrowth aquatic plants into a useable product, such as biochar, can not only provide an alternative disposal route for unwanted biomass but also produce quality value-added materials with a wide variety of applications [7, 8]. Biochar is a stable carbon-rich material that provides the ability to deal with issues of water contamination; however, biochar in powder form is very difficult to be separated from the aqueous solution in practical applications [9]. Accordingly, a solution to introduce magnetic content into the carbon phase would be a suitable strategy to deal with the separation problem of the biochar [10]. The addition of magnetic contents to the biochar leads to the creation of magnetic biochar which not only possessed excellent magnetic separation performance but also provides additional adsorption sites, and a higher surface area in comparison with the original sample [11]. The creation of traditional biochar can be achieved via a pyrolysis process which is a popular method to synthesize carbonized materials such as biomass from agriculture waste and unwanted biomass sources [12, 13]. However, the magnetic biochar can only be fabricated with the support from magnetic precursor materials as described previously in the work of Cai et al. [14] with amino-functionalized peanut hull biochar, Niu et al. [15] with Mn-Zn ferrite biochar from battery industrial waste, or Alchouron et al. [16] with Guada bamboo and iron oxide magnetic precursors.

In this work, water hyacinth representing abundant lignocellulosic biomass but also a problematic aquatic plant was collected from rivers and pond areas in the southwest of Ho Chi Minh City, Vietnam. The plant was then impregnated with cobalt sulfates under varying input concentrations and subsequently served as feedstock for pyrolysis conversion into magnetic biochar. The main objective of this work is to determine the performance of the magnetic biochars as adsorbents for the removal of Pb(II) from contaminated effluent. The adsorption isotherm and kinetics of the magnetic biochar are measured and used for the correlation of the Pb(II) uptake. Fourier transform infrared spectroscopy (FTIR), X-ray diffraction (XRD), scanning electron microscopy (SEM), surface area analysis, pore size distribution, energy dispersive spectroscopy (EDS), and magnetic hysteresis measurement were adopted to characterize the magnetic behavior of the prepared biochar.

## 2. Materials and Methods

**2.1. Materials and Chemicals.** The water hyacinth was collected from rivers and pond areas of Lai Vung district, Dong Thap province, Vietnam. Nitrogen and oxygen gas were purchased from the local manufacturing company in Vietnam (Sovigaz Vietnam Company). The chemicals of sodium hydroxide (NaOH) were supplied from Sino-pharm Chemical Reagent Co., Ltd., China. Cobalt(II) sulfate heptahydrate ( $\text{CoSO}_4 \cdot 7\text{H}_2\text{O}$ ), and lead(II) nitrates ( $\text{Pb}(\text{NO}_3)_2$ ) were purchased from Sigma Aldrich. All chemical solutions were prepared using deionized (DI) water (18.2 M $\Omega$ ), and the same DI water also was used to rinse and clean samples during the work (DI water was purchased from Vinachem chemical company). Plastic containers were purchased from Bach Khoa Chemical Company. Chemicals were used at analytical grade and without any further purification.

**2.2. Production of Water Hyacinth Magnetic Biochar.** The conversion of water hyacinth biomass into biochar is depicted in Figure 1. Briefly, the biomass was cleaned with tap water and cut into small chunks with the size of 1-2 cm long and then dried under the sun for 96 hours. The dried plant was soaked in sodium hydroxide NaOH 0.1 M at 50°C and then dried to the constant mass (Table S1 concludes the physicochemical properties of the dried water hyacinth used in this work as an input material). The final pretreatment stage includes the second drying process which happened at 105°C in an oven for 24 hours. The dried samples were then impregnated with  $\text{CoSO}_4$  solution at a varying concentration of 1, 1.5, and 2 M via magnetic stirring for 30 minutes at 45°C (mixing speed 150 rpm).

The solution of NaOH 0.5 M was added drop-wise to maintain the pH value at 10 which leads to the creation of a blue gel of  $\text{Co}(\text{OH})_2$  (mixing speed 200 rpm). In order to accelerate the impregnation reaction, the mixture containing the dried water hyacinth and the  $\text{Co}(\text{OH})_2$  solution was put under a temperature of 70°C and maintained stirring for

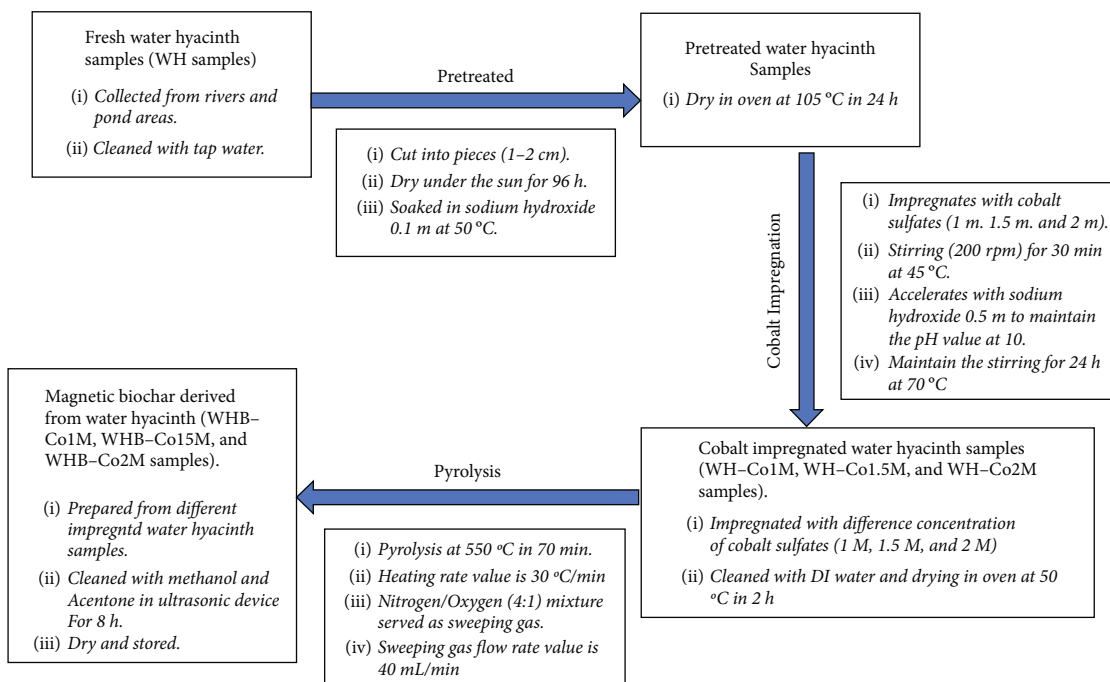
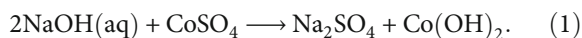


FIGURE 1: The preparation process of the magnetic biochar is derived from water hyacinth biomass.

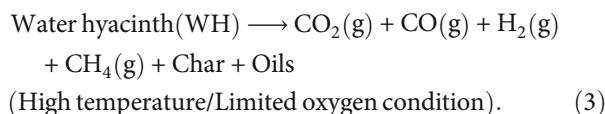
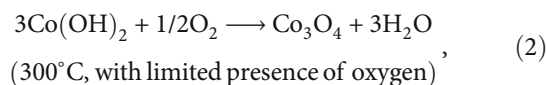
24 h (200 rpm). The reaction of the cobalt sulfate at the alkaline condition can be described as below:



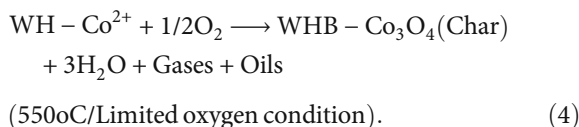
Following the impregnation process, products should include water hyacinths impregnated with various concentrations of  $\text{CoSO}_4$  which are water hyacinths impregnated with  $\text{CoSO}_4$  1 M (WH-Co1M), 1.5 M (WH-Co1.5M), and 2 M (WH-Co2M), respectively. The system we used in this work is very similar to the pyrolysis system in our previous work [17]. The carbonization of impregnated water hyacinth was carried out at 550°C (heating rate value 30°C/min) for 70 minutes. The  $\text{Co}(\text{OH})_2$  obtained in this process is in the form of blue precipitation. The layers of hydroxide and cobalt possessed residual positive charges and alternated quickly with other anions such as nitrate, carbonate, or chloride [18, 19]. Following the impregnation process, products should include water hyacinths impregnated with various concentrations of  $\text{CoSO}_4$  which are water hyacinths impregnated with  $\text{CoSO}_4$  1 M (WH-Co1M), 1.5 M (WH-Co1.5M), and 2 M (WH-Co2M), respectively. Figure S1 in the supplementary files provides more information about the pyrolysis chamber.

The mixture of nitrogen/oxygen with the ratio of 4:1 serves as sweeping gas, and the flow rate has been carefully controlled at 50 mL/min throughout the process. The use of nitrogen/oxygen mixture as the sweeping gas was crucial, which supports the cause of the creation of the  $\text{Co}_3\text{O}_4$ , reduces the tar generation, exhibits the creation of char, and saves the investment cost for running the pyrolysis process [20]. The low flow of a sweep gas maintains the limited amount of oxygen residue in the chamber. The creation of  $\text{Co}_3\text{O}_4$  from  $\text{Co}(\text{OH})_2$  can only be operated in the presence

of air and at a temperature of 300°C or above [21, 22]. The reaction below describes the synthesis of  $\text{Co}_3\text{O}_4$ :



The overall reaction would be the combination of reactions (2) and (3):



**2.3. The Batch Experiment of Lead Ion Removal.** The wastewater sample originated from an industrial circuit board manufacturer in Cu Chi Province, Ho Chi Minh City, Vietnam. All samples were collected using 10-L plastic lab containers and taken to the laboratory within two hours. The collected samples were then stored in the refrigerator for 12 hours at 10°C for metal preservation. After storage, the wastewater can be used as an influent for the process of removal of lead ions using magnetic biochar. Table S2 in the supplementary file provides characteristics of the influent used in this work, and the mentioned parameters are compared to the regulatory standard for industrial wastewater discharged.

All the experiments of lead ion removal were operated using a batch adsorption technique with the magnetic

biochar used as adsorbent (dosages value varied from 0.5 to 3 g/L). The prepared biochar then was mixed with 50 mL of influents in 250-mL digestion vessels with the adjustment of pH values at 7 using NaOH and HNO<sub>3</sub> 0.01 M. The vessels were then shaken in a mechanical shaker at 200 rpm at room temperature. At the end of the experiment, the vessels were collected and filtered to determine the concentration of Pb(II) remains in the liquid phase. The determination of Pb(II) concentration was carried out using inductively coupled plasma atomic emission spectroscopy (ICP, Aivo 200 by Perkin Elmer). All the adsorption experiments were performed in duplicate, and the average value possessed relative errors smaller than 5%. Kinetic experiments were studied by mixing 10 mg of sorbent with 50 mL of influent with a concentration of 200 mg/L at 35°C at different time intervals (0, 100, 200, and 300 min). Sorption isotherm was studied using similar experiments with 10 mg of sorbent mixed with 50 mL of influent at 25, 35, and 45°C and with different concentrations of Pb(II) (from 0 to 200 mg/L).

The adsorbed Pb(II) ( $Q_e$ , mg/g) and the removal efficiency (R, %) can be calculated using the following equations:

$$\text{The amount adsorbed Pb(II): } Q_e = \frac{(C_o - C_e) \cdot V}{m},$$

$$\text{The removal efficiency of Pb(II): } R (\%) = \frac{C_o - C_e}{C_o} \times 100, \quad (5)$$

where  $C_o$  is the initial concentration of Pb(II) in the influent (mg/L),  $C_e$  is the concentration of Pb(II) remains in the wastewater sample at equilibrium (mg/L),  $m$  is the mass of magnetic biochar used (g), and  $V$  is the volume of influent (L).

Adsorption kinetics of the lead ion removal process was performed by adopting the selected magnetic biochar samples as adsorbents for the treatment under selected conditions, and various working times varied from 0 to 300 min. The pseudo-first-order, pseudo-second-order, and Elovich models were applied to indicate the adsorption mechanism. The equations of the pseudo-first-order, pseudo-second-order, and Elovich models are described as follows:

$$\text{Pseudo - first order model : } \ln (Q_e - q_t) = \ln Q_e - k_1 t,$$

$$\text{Pseudo - second order model : } q_t = \frac{k_2 \cdot Q_e^2 \cdot t}{1 + k_2 \cdot Q_e \cdot t},$$

$$\text{Elovich model : } q_t = \frac{1}{\beta} \cdot \ln (\alpha\beta) + \frac{1}{\beta} \cdot \ln t, \quad (6)$$

where  $Q_e$  is the Pb(II) adsorption capacity at equilibrium (mg/g) and  $q_t$  is the Pb(II) adsorption capacity (mg/g) at the interval time  $t$  (min). The  $k_1$  is the pseudo-first-order rate constant (1/min) and  $k_2$  is the pseudo-second-order rate constant (g/mg.min). The initial adsorption rate is  $\alpha$  (mg/g.min), and  $\beta$  is the desorption constant (g/mg).

Adsorption isotherm of the lead ion removal process can be determined using the two-parameter models such as Freundlich and Langmuir models and three-parameter

model such as Sips model. Langmuir's model was employed to assess and calculate the adsorption behavior of the WHB-Co samples. In accordance with Wang et al. [23], the adsorbates binding to the surface of the adsorbents is mainly related to the physical forces and assumes that all adsorption sites possess an equal affinity for the sorbate. The Langmuir model can be described as:

$$\text{Langmuir isotherm : } Q_e = \frac{Q_{\max} \cdot K_L \cdot C_e}{1 + K_L \cdot C_e}, \quad (7)$$

where  $C_e$  is the equilibrium concentration (mg/L),  $Q_{\max}$  is the maximum adsorption capacity of the adsorbents (mg/g), and  $K_L$  is the equilibrium coefficient of the Langmuir model (L/mg).

Freundlich isotherm model can be adopted to evaluate the adsorption on diverse surfaces and indicates the stronger binding sites that are occupied first during the adsorption process. The model can be applied to multilayer sorption to describe the relationship between the adsorbent and the sorbate [24]. The Freundlich model can be described as:

$$\text{Freundlich isotherm : } Q_e = K_F C_e^{1/\eta F}, \quad (8)$$

where  $C_e$  is the equilibrium concentration (mg/L),  $\eta F$  is the exponent of the Freundlich model, and  $K_F$  is the Freundlich model coefficient ( $[L^{\eta F} \cdot \text{mg}^{(1-\eta F)}] / \text{g}$ ).

On the other hand, the Sips model provides the prediction of an adsorption process in a heterogeneous system with monolayer adsorption associated with the Langmuir model and prevents the rise of adsorbate concentration associated with the isotherm described by the Freundlich model. The Sips adsorption isotherms can be determined following the equation:

$$\text{Sips isotherm : } \frac{Q_e}{Q_m} = \frac{K_s \cdot C_e^n}{1 + K_s \cdot C_e^n}, \quad (9)$$

where  $Q_m$  is the maximum uptake (mg/g),  $K_s$  is the isotherm constant (L/mg) <sup>$n$</sup> , and  $n$  is the heterogeneous value.

All the isotherm models were also recorded and verified with the sum of squares errors and correlation coefficient value. Nonlinear equations of Langmuir, Freundlich, and Sips models were used to fit the experimental data by adopting the least square method.

**2.4. Material Characterization and Analysis Procedure.** Different characterization methods were adopted to study the affection of initial magnetic precursor concentration on the creation of the magnetic biochars. All the measurements were carried out in duplicate and repeatable to strengthen the quality of the work. Average values and standard deviations are presented along with figures throughout the work. Elemental analysis of the water hyacinth biomass and the as-prepared magnetic biochar was carried out using the elemental analyzer Fison' EA 1108 CHNS, according to the ASTM 5291-96. The proximate analysis includes the measurement of moisture, volatile matter, carbon content, and ash contents and was carried out following the standard

methods. Both proximate and elemental analyses possessed deviation values less than 5%.

The microstructure and morphology of each sample were examined by SEM Hitachi-S4800 type 2 with Thermo NORAN NSS EDS: cold field emission electron gun. The resolution of the machine was 1 nm at 1 kV and 1.4 nm at 15 kV, with magnifications ranging from 20 to 800,000 times. In addition, the STEM detector showed the best performance at 200 kV acceleration voltage. The as-prepared magnetic biochar sample was coated with gold for high conductivity and a high-quality image. Functional groups and their interaction with the as-prepared magnetic biochars were determined using FTIR Aplphe II by Bruker in the scanning range of 4000 to 600  $\text{cm}^{-1}$ . The phases and crystalline structure analysis were examined by XRD Malvern Panalytical, with X'pert pro-MRD, using copper (Cu) K (alpha) radiation.

The surface area of each sample was determined by the Brunner-Emmet-Teller (BET) method, and the sample porosity was analyzed by porosimetry of the adsorption/desorption isotherms using nitrogen and argon at 77 K. All samples were degassed at 300°C for 2 h. Both of the measurements are carried out by porosimetry and accelerated surface area system ASAP 2420 equipment by Micromeritics.

Thermogravimetric analysis was performed using TG/DTA analyzer from Perkin Elmer Diamond. The heating rate was set to 10°C/min in the temperature range of 30 to 900°C with nitrogen flow (100 mL/min) to determine the thermal properties of the as-prepared magnetic biochar and therefore indicate the role of magnetic precursor added to the biochar via the preparation steps.

Inductively coupled plasma (ICP, Aivo 200 by Perkin Elmer) equipment was used to determine the concentration of heavy metals in the effluent. The applied plasma gas was at 15 L/min, the auxiliary gas was at 1.4 L/min, carrier gas was at 1.5 L/min, and the pump speed was at 15 rpm.

The magnetic measurement was carried out using a vibrating sample magnetometer (VSM) (BHV-55, Riken, Japan). The magnetic field was set in the range of 0 to 3.0 T, while the scope of the magnetic moments was at  $10^{-2}$ -300 emu (sensitivity:  $5 \times 10^{-5}$  emu). The working temperature was set in the range of 0 to 700°C.

### 3. Results and Discussions

#### 3.1. Characterization of the Magnetic Biochars

**3.1.1. The Creation of the Cobalt Magnetic Biochar.** The physicochemical properties and the mass yield of the as-prepared magnetic biochar are summarized in Table 1. As observed, the magnetic biochar mass yield is increased (from 42.08% to 42.71% at max yield) as the concentration of magnetic precursors was increased along with the samples (1 M, 1.5 M, and 2 M of cobalt sulfate were added to the dried biomass). Following the proximate analysis, the moisture content in all samples was reduced after the pyrolysis process (from 6.34% in the WHB-Co1M to 6.15% in the WHB-Co2M). The changes in the moisture content of the WHB-Co1M, WHB-Co1.5M, and WHB-Co2M samples

are small and depend on the extent of the hydrophobicity phase in the materials.

The fixed carbon content of magnetic biochar decreased slightly from 20.56% in WHB-Co1M to 20.49% in WHB-Co2M. It is clear that the fixed carbon content increases when the concentration of the cobalt precursor was increased. On the other hand, the ash content in the magnetic biochar samples is composed of inorganic elements that remained after the pyrolysis process and slightly increases from 21.57% in the WHB-Co1M to 21.71% in the WHB-Co2M. The difference in volatile compounds content is also indicated and reflected in only small changes (51.53% in the WHB-Co1M, 51.57% in the WHB-Co1.5M, and 51.64% in the WHB-Co2M). Following the elemental analysis, the carbon content decreases from 43.88% in the WHB-Co1M to 42.74% in the WHB-Co2M. The amount of carbon was expected to be lost due to contact with the oxygen in the sweeping gas during the heating process, which may result in partial calcination. In this work, the obtained carbon content and hydrogen content via the elemental analysis are lower than expected.

The mentioned fact can be explained by the presence of a limited volume of oxygen during the pyrolysis process. Although the contact with oxygen during the pyrolysis is controlled (sweep gas ratio is 4:1, the flow rate of 50 mL/min) and the volume of oxygen joined in available reactions is small (10 mL/min), that was still sufficient for the small reduction in fixed carbon content in magnetic biochar samples. Similar results were found in other works of greenhouse crop [24], corn stalk [25], and rice husk [26] which indicate the affection of pyrolysis temperature at 550°C to the change in both elemental analysis results and proximate analysis results. According to the results concluded in Table 1, the introduction of cobalt precursors at different concentrations did not affect the physicochemical properties of the final products afterward, while the pyrolysis temperature and the oxygen content from the sweeping gas-only may cause the smallest change in both the content of ash and hydrocarbon elements.

**3.1.2. Chemical Structure and Phase Analysis.** Fourier transform infrared spectroscopy (FTIR) was used to determine the chemical structure of the magnetic biochars in this work. During the pyrolysis process, temperature, heating time, and the ratio of cobalt precursors on biomass affected the properties of the produced samples. In most cases, the temperature is the most important factor and directly shows its influence on the magnetic biochar substance [27]. However, the results obtained in this work indicate how the initial concentration of magnetic precursors affects the chemical structure of the as-prepared magnetic biochars. In Figure 2(a), we observe sharp peaks at around 577, 604, and 597  $\text{cm}^{-1}$  together with peaks at 615, 627, and 631  $\text{cm}^{-1}$  for WHB-Co1M, WHB-Co1.5M, and WHB-Co2M, respectively. Those mentioned spectrums are associated with the  $(\text{Co}^{3+})\text{-O}$  (in an octahedral hole) and the  $(\text{Co}^{2+})\text{-O}$  (in a tetrahedral hole) vibration [28, 29].

The phenomena also confirm the existence of the magnetic cobalt that has been successfully impregnated on the biochar following the preparation steps in this work. These

TABLE 1: Physicochemical properties and mass yield of the magnetic biochar. The obtained data values are the mean  $\pm$  standard deviation of triplicate experiments.

Analysis	Samples			
	Content (%)	WHB-Co1M	WHB-Co1.5M	WHB-Co2M
Proximate analysis	Moisture	6.34 $\pm$ 0.04	6.22 $\pm$ 0.02	6.15 $\pm$ 0.03
	Volatile	51.53 $\pm$ 0.28	51.57 $\pm$ 0.32	51.64 $\pm$ 0.35
	Ashes	21.57 $\pm$ 0.20	21.65 $\pm$ 0.18	21.71 $\pm$ 0.25
	Fixed carbon	20.56 $\pm$ 0.10	20.56 $\pm$ 0.10	20.49 $\pm$ 0.10
Ultimate analysis	C	43.88 $\pm$ 0.19	42.76 $\pm$ 0.18	42.74 $\pm$ 0.18
	H	0.85 $\pm$ 0.05	0.80 $\pm$ 0.04	0.82 $\pm$ 0.05
	O	15.85 $\pm$ 0.16	16.01 $\pm$ 0.18	16.42 $\pm$ 0.18
	N	0.67 $\pm$ 0.06	0.73 $\pm$ 0.06	0.72 $\pm$ 0.05
Mass yield (%)		42.08	42.34	42.71

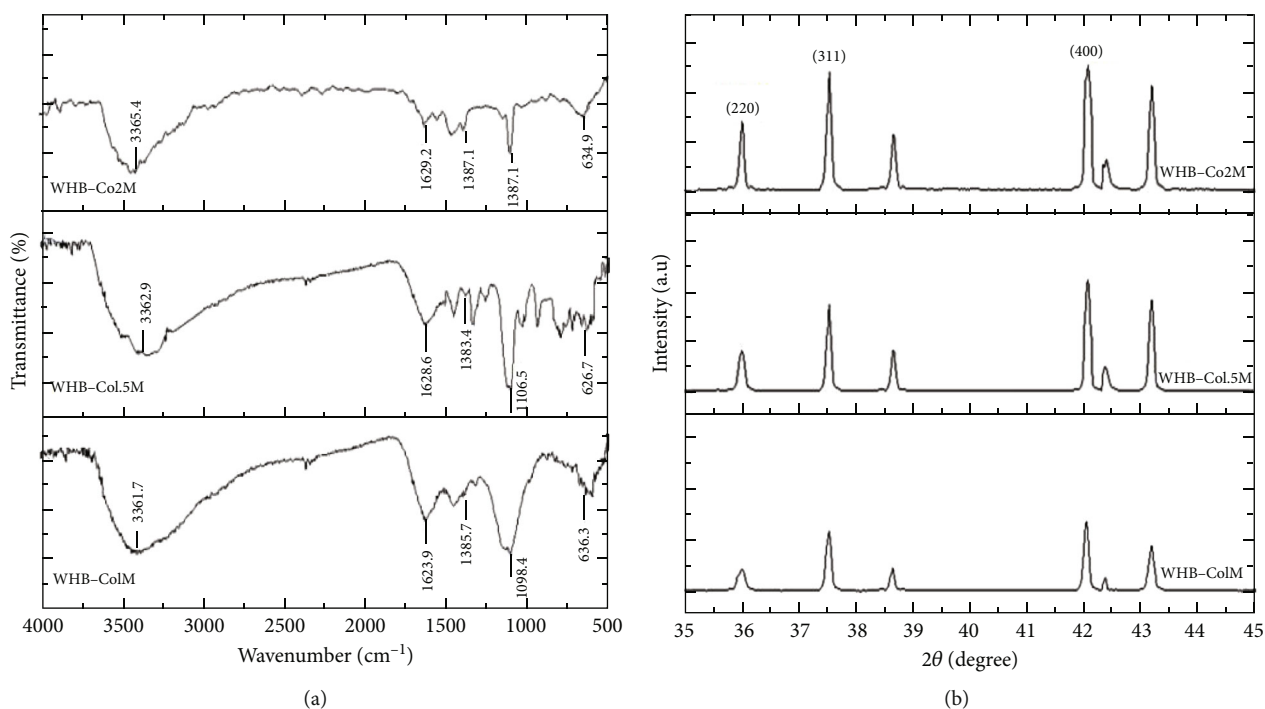


FIGURE 2: The FTIR spectrum (a) and the XRD patterns (b) for the different samples of cobalt magnetic biochars.

peaks of about 1099 to 1106  $\text{cm}^{-1}$  are attributed to the stretching vibrations of C-O and carbonate anions that occurred during the pyrolysis process. Those peaks at round 1383 to 1387  $\text{cm}^{-1}$  indicate the C-H deformation vibration of hemicellulose (at 1383  $\text{cm}^{-1}$ ), lignin (at 1387  $\text{cm}^{-1}$ ), and cellulose (at 1385  $\text{cm}^{-1}$ ) content in all three samples, and similar results can be found within the work of Zhang et al. [30] and Khandalou et al. [31]. Broad peaks at around 3361, 3362, and 3365 as well as those at 1623, 1628, and 1629  $\text{cm}^{-1}$  would belong to the stretching of the O-H bond which is assigned to the content of water in the sample of WHB-Co1M, WHB-Co1.5M, and WHB-Co2M, respectively. The FTIR analysis successfully indicates the changes in the chemical

structure of each magnetic biochar sample under the influences of the initial concentration of magnetic precursors added during the preparation steps, previously. Accordingly, the difference in cobalt precursors does not dramatically affect the nature of the final product, but most likely confirms a successful preparation process.

For a more in-depth investigation of the phase properties and crystallinity of the prepared magnetic biochars, X-ray diffraction (XRD) analyses were conducted. Figure 2(b) concludes the XRD patterns of the three different samples with a series of diffraction peaks at the  $2\theta$  degrees of 32.69, 37.21, 43.77, and 63.58 which can be assigned to the plane of (220), (311), (400), and (440). Accordingly, the XRD

patterns we obtained in this work are well uniformed in comparison to each other and similar to values reported for  $\text{Co}_3\text{O}_4$  spinel cubic in the JCPDS card number 42-1467 [32].

As we can observe in Figure 2(b), the modification of cobalt precursor concentration indicates small changes to the creation of the final samples, including that the weak intensity of those peaks at around  $32.69$  ( $220$ ) at  $2\theta$  degrees is getting smaller and weaker from WHB-Co1M to WHB-Co2M. In the case of the WHB-Co1M sample, the ( $220$ ) peak was small and broad which indicates poor magnitude properties and an amorphous phase. For the case of WHB-Co1.5M and WHB-Co2M samples, peaks at around  $32.69$  ( $220$ ) were also very low and can be explained by the influence of pyrolysis temperature on the size distribution of nanocrystal materials in the sample. The orientation of  $\text{Co}_3\text{O}_4$  strongly depends on the pyrolysis temperature which means the cobalt contents increase in nanocrystalline size for the cost of the amorphous phase at the pyrolysis temperature of  $550^\circ\text{C}$  [33].

The diffraction peaks at  $37.21$   $2\theta$  ( $311$ ) which are the main peaks of  $\text{Co}_3\text{O}_4$  show small sharp peaks with similar intensity for the three samples. Therefore, there are only very thin crystalline single phases of the cubic crystal structure that are formed. The difference in peak intensity at this orientation is not much different. The peak found in the WHB-Co2M sample XRD pattern appears to be better and clearer in comparison with the other samples due to its highest peak intensity. The same phenomena were found at the peaks of  $43.77$  and  $63.58$  of  $2\theta$  degrees, and no other peaks for impurities were detected in these patterns. All the carbon content included in the XRD analysis was at the amorphous phase due to their broad peak around  $25$  of  $2\theta$  degrees. Similar confirmations can also be found in the work of Yang et al. [34], Tian et al. [35], and Kemmou et al. [36]. The results obtained via XRD analysis can determine the successful preparation of magnetic biochar with the support of cobalt precursors. However, the change in the concentration of the used precursors reflects only small differences between the peak intensity of three magnetic biochar samples.

**3.1.3. Morphological Analysis.** The morphology of these as-prepared magnetic biochar samples including dried biomass sample, alkaline-treated sample, biochar sample, WHB-Co1M, WHB-Co1.5M, and WHB-Co2M is shown in Figure 3. As we can observe, Figures 3(a) and 3(b) show the morphological image of dried biomass and alkaline-treated samples, respectively. The surface of the biomass was changed and got rougher after the alkaline treatment process, and the use of the alkaline solution is meant to remove hemicellulose, lignin, and some other organic compounds that may contact with the dried biomass from previous preparation steps [37, 38]. The morphology of the alkaline treated sample in Figure 3(b) indicates the successful solubilization of hemicellulose and lignin with a notable amount as well as enhancing the porosity and surface area of cellulosic content in the sample [39, 40].

Figure 3(c) indicates a clear image of the produced biochar in similar sizes and shapes. However, the morphology of the cobalt impregnated biochar samples reveals a very dif-

ferent story and confirms that the concentration of magnetic precursors is associated with the loading of the metal content during pyrolysis. In Figure 3(d), the WHB-Co1M provides the morphology of a surface with  $\text{Co}_3\text{O}_4$  anchored. It is clear that the  $\text{Co}_3\text{O}_4$  particles are scattered on a rough surface of the biochar and were not uniformed, and the creation of a dense surface was not achieved. Figure 3(e) describes a more transparent surface of sample WHB-Co1.5M with more particles of  $\text{Co}_3\text{O}_4$  can be recognized. The quantity of cobalt content increases clearly. There were some pore-shaped  $\text{Co}_3\text{O}_4$  particles from the size of  $100$  nm that can be found uniformly anchored to the sample and covered across the surface of the biochar.

In the case of the WHB-Co2M sample, Figure 3(f) shows the morphology of a dense and well-covered surface of biochar with the size, and the form of the created cobalt(II, III) oxides is not so different in comparison with those in the WHB-Co1M sample in Figure 3(e). The small images on the left corner indicate a clearer state of the sample; uniformed pore-shaped particles of  $\text{Co}_3\text{O}_4$  cover the biochar surface and almost create a dense layer with similar morphology.

The increase of magnetic precursor concentration extends the loading of the metal on the biochar, whereas the creation of  $\text{Co}_3\text{O}_4$  was at around  $300^\circ\text{C}$  and the completed magnetic biochar was at  $550^\circ\text{C}$ . Consequently, WHB-Co2M seems to have better properties with larger surface properties, higher porosity, and thermal stability compared to the other two. The discussion about porosity, surface, and other properties of magnetic biochars can be confirmed later in this work. Similar results were obtained in the work of Liu et al. [41], Wang et al. [42] from a bloom-forming, and Sewu et al. [43]; the effects of the initial concentration of the magnetic precursors on the metal loading on the biochar are confirmed following the results presented in this work. The small EDS graph at the corner of Figures 4(d), 4(e), and 4(f) confirms the successful creation of the cobalt impregnated biochar in all three samples. The confirmation of the successfully impregnation process of cobalt content is also supported via the EDS analysis in Figure S2 in the supplementary file.

**3.1.4. The Magnetic Hysteresis and Thermal Properties of the Impregnated Magnetic Biochar.** The difference in cobalt content for each magnetic biochar sample would directly affect its properties and performance. In this way, the efficiency of magnetic biochars can be determined through the study of their surface, thermogravimetric and magnetic properties. Figure 4 shows the magnetic hysteresis loop and the thermal gravimetric analysis results of WHB-Co1M, WHB-Co1.5M, and WHB-Co2M samples, respectively.

As indicated in Figure 4(a), the WHB-Co2M sample possesses the highest saturation magnetization value ( $14.74$  emu/g), followed by the WHB-Co1.5M ( $12.51$  emu/g) and the WHB-Co1M ( $11.77$  emu/g). All three samples react positively with the applied magnetic field varied between  $10$  and  $-10$  kOe and can be easily separated from the aqueous phase by a magnet.

The input of different cobalt precursor concentrations from the previous preparation steps strongly affects the

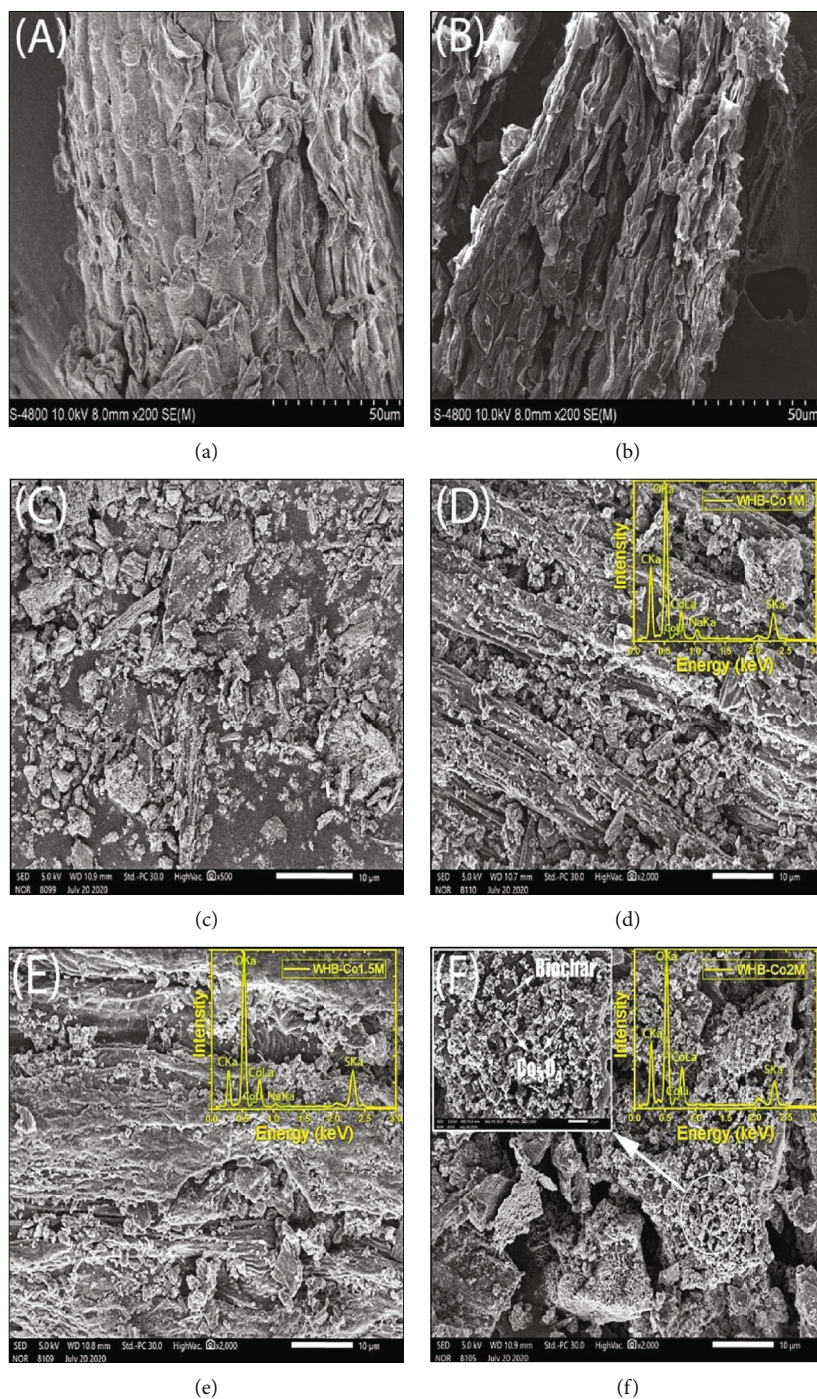


FIGURE 3: SEM images of (a) dried biomass sample; (b) alkaline-treated biomass sample; (c) water hyacinth biochar: WHB; (d) biochar WHB-Co1M sample; (e) biochar WHB-Co1.5M sample; and (f) biochar WHB-Co2M sample (with higher calibration image attached).

magnetic properties of the magnetic biochars. The cobalt loading during pyrolysis was crucial in this case, where the higher cobalt content in the magnetic biochar provides better magnetization saturation. The cobalt content can be determined using the digestion method, and the results are given in Table 2.

With the largest surface area ( $192 \text{ m}^2/\text{g}$ ) and pore volume ( $0.126 \text{ cc/g}$ ), the WHB-Co2M sample also includes the highest cobalt content ( $38.94 \text{ mg/g}$ ) which indicates the great

saturation magnetization value over the other two samples. This may be explained following the thermogravimetric analysis illustrated in Figure 4(b). Light hydrocarbon components and moisture were removed at temperatures ranging from  $100^\circ\text{C}$  to  $150^\circ\text{C}$ . At  $300^\circ\text{C}$  with only 15-20% weight loss,  $\text{Co}(\text{OH})_2$  was converted to  $\text{Co}_3\text{O}_4$  with the support of oxygen from the pumped ambient air ( $45 \text{ mL/min}$ ) which also means the creation of the magnetism cobalt occurred before the completed creation of the biochar at



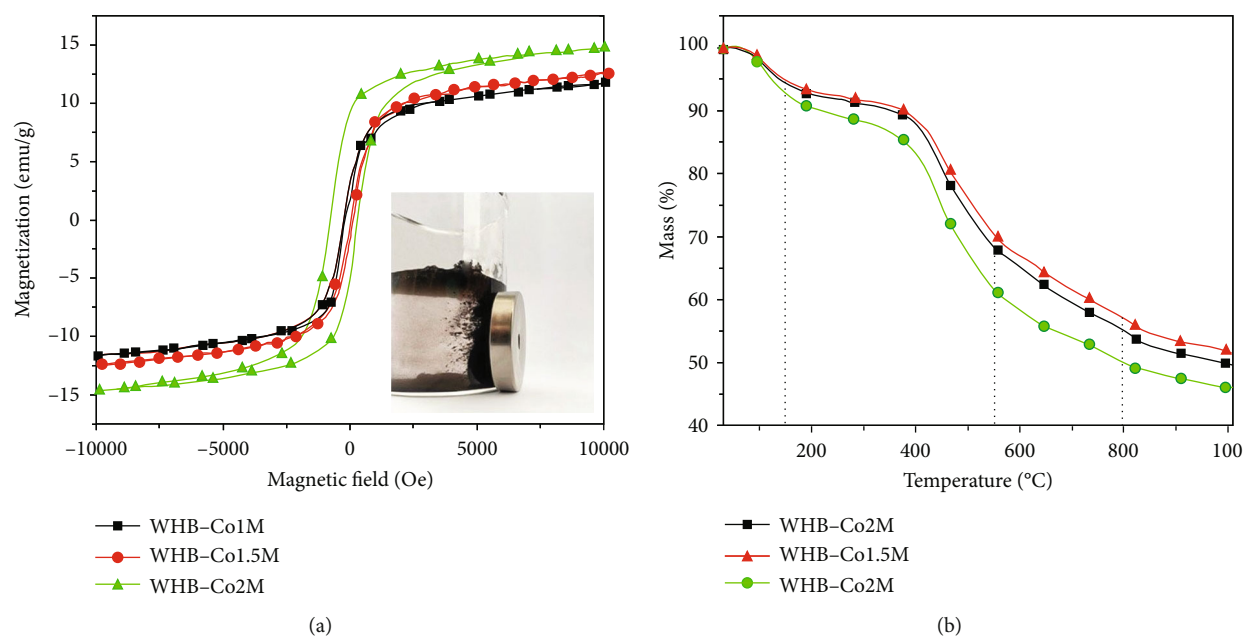


FIGURE 4: The magnetic hysteresis loop (a) and the thermogravimetric-TGA analysis (b) of the magnetic biochar samples.

TABLE 2: Surface area analysis and cobalt content in the prepared samples.

Samples	WHB-Co1M	WHB-Co1.5M	WHB-Co2M
$S_{BET}$ ( $m^2/g$ )	137	167	192
Pore diameter (nm)	1.2	1.2	1.2
Pore volume (cc/g)	0.086	0.118	0.126
Cobalt content (mg/g)	31.26	36.78	38.94

550°C with more than 70% mass weight remains for all samples. The large surface area and pore-rich structure of the biochar provide a notable adsorption capacity of metal which resulted in the higher cobalt content included in the sample treated with the higher input magnetic precursor concentration (WHB-Co2M > WHB-Co1.5M > WHB-Co1M) [44]. In comparison with the work of Ouyang et al. [45] and Han et al. [46], the results obtained in this work provide the homogeneous confirmation of the relationship between the metal loading on the biochar and the metal concentration in the magnetic precursor solution. In that manner, the WHB-Co2M sample is derived from the preparation process including the higher concentration of the magnetic precursor solution, and provided not only a larger surface area, but also higher thermogravimetry property, and higher magnetization saturation than the other samples. Not only that, the fact that the addition of metal sites to the biochar has the potential to extend the surface area, the pore volume, and the sorption of the biochar has been confirmed by Chen et al. [47].

### 3.2. The Removal of Lead Pb(II) from Industrial Wastewater

3.2.1. Kinetics Study and the Effects of Adsorption Times on the Removal Efficiency. The original concentration of 95 mg/L of

Pb(II) of the influent (as described in Table S1) would be completely removed in about 7-10 minutes so that in these batch experiments, longer adsorption times were used (0 to 300 mins). Figure 5(a) determines the effects of adsorption times on the removal efficiency of the process. The adsorption of lead ions Pb(II) on the prepared magnetic biochars was fast and reached equilibrium in 100 mins.

All three magnetic biochar samples, WHB-Co1M, WHB-Co1.5M, and WHB-Co2M, indicate a fast rate adsorption process with more than 80% of the Pb(II) and were removed in the first 75 mins; the removal rate then slowed down apparently until the equilibrium was achieved after 100 mins and stable to the end of the process. The adsorption in the early stage of this work can be attributed to reactions such as electrostatic and ion exchange which were reported to reach equilibrium quickly after a few minutes [48, 49]. The WHB-Co2M sample provided the highest removal efficiency (up to 85%) after 100 mins, at room temperature (35°C).

It is reasonable to argue that the higher surface area (192  $m^2/g$ ) and high porosity (0.126 cc/g pore volume) of the WHB-Co2M sample provide the ability to adsorb more Pb(II) ions. In addition, results in Table 3 also showed that the faster mass transfer during the adsorption is governed by an excellent pore-filling mechanism [50, 51].

Figures 5(b) and 6(c) and 6(d) determine the Pb(II) adsorption kinetic of the WHB-Co1M, WHB-Co1.5M, and WHB-Co2M magnetic biochar sample that were used as adsorbents in this work, respectively. The mononuclear and binuclear adsorption were described using the pseudo-first-order and pseudo-second-order models in a solid-solution system. The Elovich model was also applied to evaluate the contribution of desorption throughout the process. The calculated kinetic parameters from the three models are listed in Table 3.

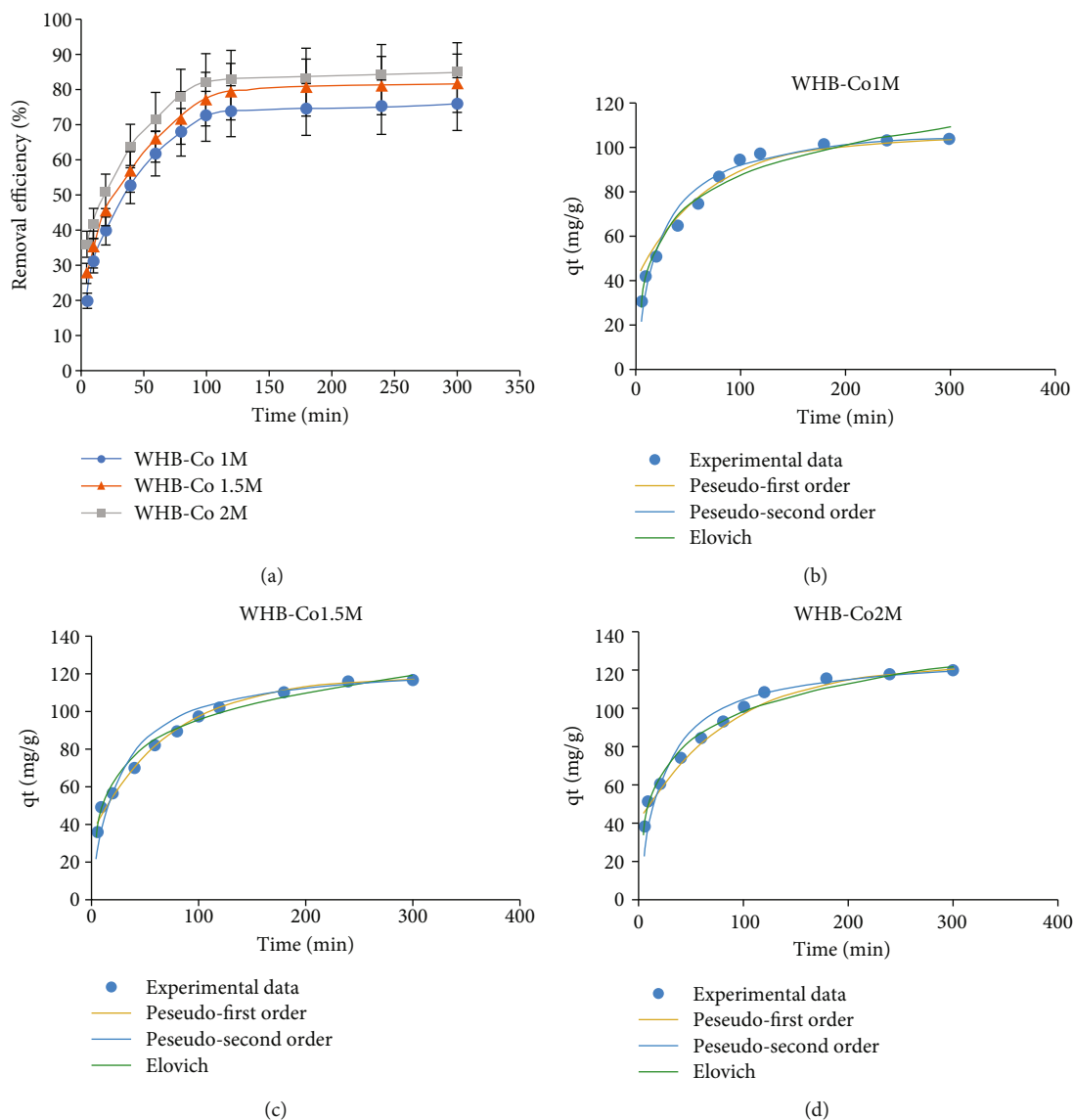


FIGURE 5: Plots of (a) the removal efficiency versus the adsorption time and the adsorption kinetics for Pb(II) on WHB-Co1M (b), WHB-Co1.5M (c), and WHB-Co2M (d) sample. The adsorption kinetics data were calculated following the pseudo-first-order, pseudo-second-order, and Elovich models.

TABLE 3: The kinetic parameters of magnetic biochar sample adsorption.

Samples	$Q_e, \text{exp}$ (mg/g)	Pseudo-first order			Pseudo-second order			Elovich		
		$Q_e$ (mg/g)	$K_1$ (1/min)	$R^2$	$Q_e$ (mg/g)	$K_2$ (g/mg.min)	$R^2$	$\beta$ (g/mg)	$\alpha$ (mg/g.min)	$R^2$
WHB-Co 1M	105	64.482	0.0149	0.965	112.359	0.0004	0.997	0.049	16.170	0.972
WHB-Co 1.5M	119	83.948	0.0136	0.997	126.582	0.0003	0.995	0.047	19.542	0.986
WHB-Co 2M	125	83.948	0.0117	0.985	129.870	0.0003	0.995	0.046	21.273	0.984

In the case of the WHB-Co1M sample (described in Figure 5(b)), the correlation coefficient value ( $R^2 = 0.9972$ ) of the pseudo-first-order model is higher than those of the pseudo-first-order model ( $R^2 = 0.9658$ ) and the Elovich model ( $R^2 = 0.9722$ ). Furthermore, the calculated  $q_e$  value (112.3595 mg/g) from the pseudo-second-order model was also closer to the  $Q_e$  value (105 mg/g) from the experiment

in comparison with the  $Q_e$  value (64.4828 mg/g) calculated from the pseudo-first-order model. As for the case of WHB-Co1.5M (described in Figure 5(c)), the adsorption behavior occurred with the correlation coefficient value ( $R^2$ ) followed the order of pseudo-first order ( $R^2 = 0.9972$ ), pseudo-second order ( $R^2 = 0.9954$ ), and Elovich ( $R^2 = 0.9856$ ). The obtained data indicate that the first order would be the most suitable

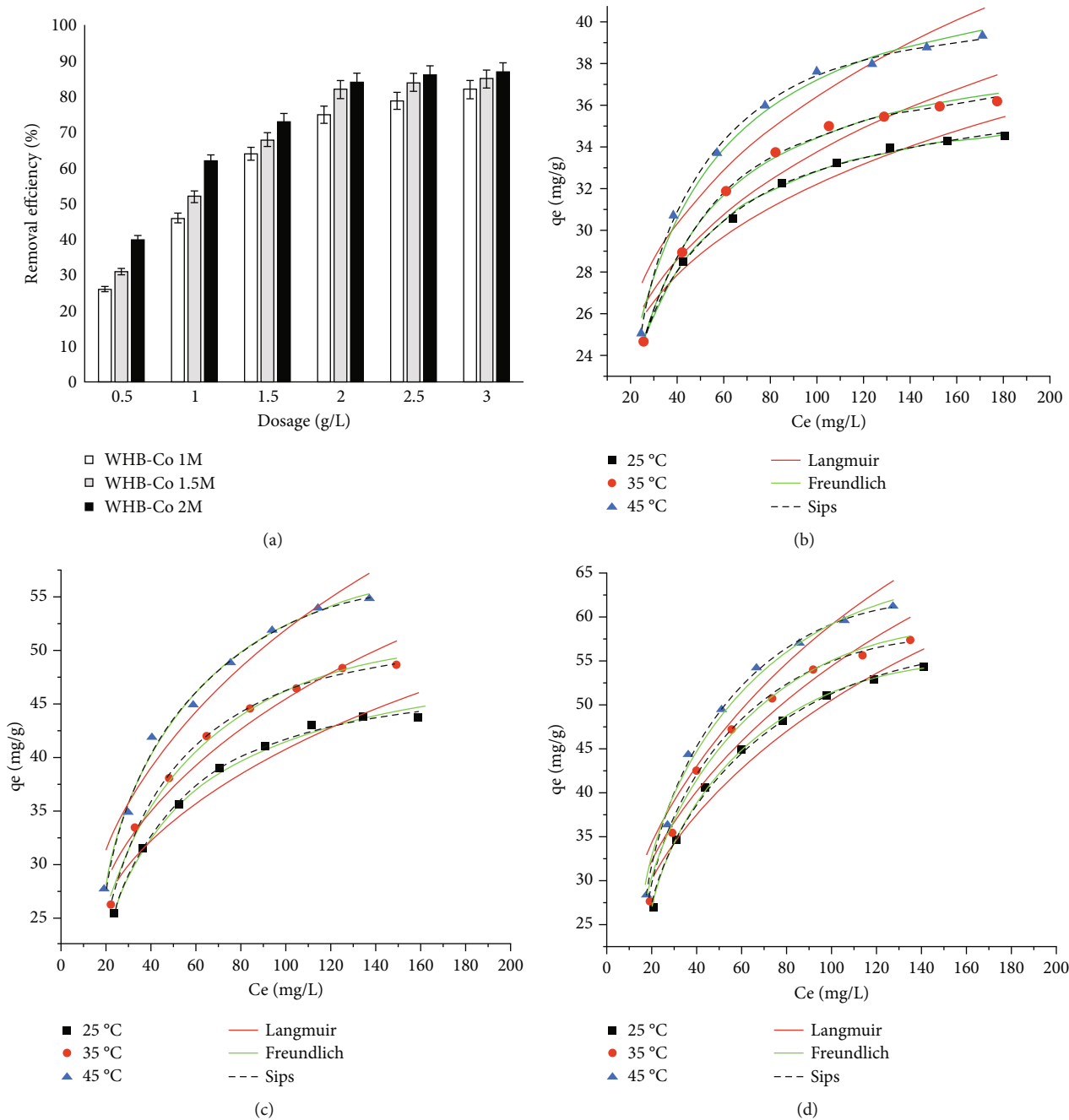


FIGURE 6: Effects of adsorbent dosage on the removal efficiency (a), the adsorption isotherm for Pb(II) on WHB-Co1M (b), WHB-Co1.5M (c), and WHB-Co2M (d) sample.

model for the description of the adsorption kinetics using the WHB-Co1.5M sample as an adsorbent. The WHB-Co2M adsorption kinetic is described in Figure 5(d); the pseudo-second-order model fitted best to the experimental data with the higher correlation coefficient value ( $R^2 = 0.9959$ ) in comparison with those calculated from the pseudo-first order ( $R^2 = 0.9856$ ), and Elovich ( $R^2 = 0.9846$ ). The rate constant of the pseudo-second-order model showed that the WHB-Co1M sample possessed a faster adsorption rate than the WHB-Co2M. It is reasonable to confirm that the pseudo-second order is the most suitable model to describe the

adsorption kinetic of Pb(II) on the magnetic biochar samples of WHB-Co1M and WHB-Co2M, while the WHB-Co1.5M is more suitable for the adsorption kinetics described by the pseudo-first order. This result also indicates the domination of chemisorption over the diffusion during the adsorption process [52, 53].

3.2.2. *The Adsorption Isotherm and the Influence of Adsorbent Dosage.* The dosage of adsorbent plays a crucial role that greatly influences the adsorption process, due to its affection for the available adsorption sites. The

TABLE 4: Langmuir, Freundlich, and Sips isotherm constants for the adsorption of Pb(II) on the magnetic biochar sample.

Temperature		WHB-Co 1M			WHB-Co 1.5M			WHB-Co 2M		
		25°C	35°C	45°C	25°C	35°C	45°C	25°C	35°C	45°C
Langmuir	$Q_m$ (mg/g)	37.173	39.825	43.555	51.156	57.437	65.577	65.614	69.792	75.530
	$K_L$ (L/mg)	0.0776	0.0655	0.0587	0.0428	0.0401	0.0388	0.0353	0.0362	0.0361
	$R^2$	0.998	0.997	0.993	0.995	0.995	0.994	0.997	0.995	0.993
Freundlich	$K_F(L^{nF} \cdot mg^{1-nF})/g$	15.432	14.620	14.353	12.269	12.131	12.245	11.402	11.924	12.204
	$\eta F$	6.2423	5.4994	4.9386	3.8447	3.5018	3.1994	3.0923	3.0374	2.9185
	$R^2$	0.952	0.935	0.925	0.939	0.947	0.957	0.956	0.949	0.945
Sips	$n$	0.947	1.126	1.296	1.199	1.214	1.091	1.196	1.262	1.300
	$Q_m$ (mg/g)	37.492	38.773	41.255	48.436	53.807	63.259	61.031	63.633	67.815
	$K_S$ (L/mg) <sup>n</sup>	0.090	0.045	0.024	0.024	0.022	0.030	0.021	0.018	0.016
	$R^2$	0.998	0.998	0.997	0.997	0.997	0.995	0.999	0.998	0.998

determination of adsorption equilibrium for all magnetic biochar samples in this work includes 24-h adsorption time, and the relationship between adsorbent dosage and the removal efficiency of this work are described in Figure 6(a), while the sorption isotherm of each magnetic biochar sample which was used as adsorbent would be studied using the two-parameter (Langmuir and Freundlich) and three-parameter (Sips) isotherm models.

As observed in Figure 6(a), the plot indicates two different areas, whereas the first area shows that the removal efficiency of all three magnetic biochar samples was significantly increased (from 27% to 63% with WHB-Co1M, 32% to 67% with WHB-Co1.5M, and 41% to 72% with WHB-Co2M sample) as their dosage increase from 0.5 g/L to 1.5 g/L for all three samples. The second area indicates the removal efficiency of the work with a smaller change, with the adsorbent dosage increase from 2 to 3 g/L for all three samples and the efficiency increase with a slower rate (from 73% to 80% with WHB-Co1M, from 80% to 83% with WHB-Co1.5M, and 82% to 85% with WHB-Co2M sample). Completed removal was not yet reached due to the lack of adsorption sites from all three applied magnetic biochar samples, and all active sites would be fully occupied by the Pb(II) during the process [54]. The result obtained in this part suggests that the higher Pb(II) removal percentage would be achieved with a higher adsorbent dosage, thanks to its additional active sites.

The isotherm study includes a 24-h process with the adsorbent dosage of 2 g/L, and the concentration of Pb(II) in the influent varied from 0 to 200 mg/L. Experiments were carried out under three different temperatures to determine the effect of working temperature throughout the adsorption process. According to the acquired correlation coefficient value ( $R^2$ ) from each sample, the Langmuir and Sips models fitted the data better than the Freundlich model, regardless of the adsorption temperatures. Table 4 summarizes the isotherm parameters of Langmuir, Freundlich, and Sips models for all magnetic biochar samples. Since the Sips isotherm model is a hybrid adsorption model and also fitted best to all magnetic biochar samples applied in this work, the

obtained result indicates that both the monolayer and multilayer adsorption contribute to the removal of Pb(II). The values of the Sips exponent ( $n$ ) described the adsorption mechanism which is toward the heterogeneous or homogeneous; for a homogeneous adsorption system, the  $n$  value should be equal to 1. However, the data in Table 4 indicates that only the adsorption happened with the WHB-Co1M sample at 25°C provided the Sips exponent value below 1 ( $n = 0.9472$ ), and other cases show opposite results ( $n > 1$ ) which indicates the existence of heterogeneous adsorption mechanisms [55].

According to Table 4, the Sips exponent value ( $n$ ) increases with the increase of working temperature which reveals that at higher temperatures, the adsorption process is more heterogeneous [56]. On the other hand, the lowest adsorption capacity calculated using the Sips model was 37.392 mg/g and was recorded at 25°C with a WHB-Co1M sample, while the highest one was 67.815 mg/g with a WHB-Co2M sample at 45°C (this fact is fitted to all three applied magnetic biochar samples). This result indicates that the adsorption capacity of all three magnetic biochar samples increases following the increase in temperature.

The Langmuir Pb(II) adsorption capacity of water hyacinth magnetic biochars from this work can also be used to compare the performance of various adsorbents. The maximum uptake capacity for WHB-Co1M, WHB-Co1.5M, and WHB-Co2M was 43.55, 65.57, and 75.53 mg/g at 45°C, respectively. The adsorption capacity for Pb(II) with other carbon-based adsorbents has been reported as 99.85 mg/g with modified sewage sludge biochars [57], 45.70 mg/g with magnetic energy cane biochar [58], or 66.23 mg/g with the sugarcane bagasse treated with  $H_3PO_4$  and pyrolyzed at 400°C [59]. Table S3 in the supplementary file concludes with more comparison references [60–62] for the adsorption performance of Pb(II) with different applied adsorbents.

The adsorption mechanism of Pb(II) using magnetic biochars derived from water hyacinth can be described by both chemical and physical adsorption. As evidenced from the SEM micrograph and BET measurement, the high surface area and highly pore structure of the WHB-Co2M

provide more active adsorption sites that benefit the adsorption on its surface. As the pH value in this work is controlled 7, the results obtained from kinetic experiments indicate that the fast early adsorption stage (initial stage) can be attributed to the electrostatic attraction and ion exchange, and the removal capacity of Pb(II) depends on chemical adsorption rather than physical adsorption. It is reasonable to claim that the adsorption that happened in this work could be related to many other mechanisms such as Van der Waal forces, hydrophobic force, and  $\pi$ - $\pi$  interaction. Furthermore, the isotherm experiment provides insight into the monolayer and multilayer adsorption on the heterogeneous surface.

#### 4. Conclusion

In this work, the preparation and characterization of cobalt impregnated water hyacinth magnetic biochars via a modified pyrolysis process were successfully carried out. The role of the impregnated cobalt (II, III) oxides on biochars is confirmed following the described methods, which mainly focus on the difference in cobalt sulfate concentration throughout the preparation for the final products. The WHB-Co2M sample was found to be the most effective adsorbent for the removal of lead ions in industrial wastewater, thanks to its high porosity (0.126 cc/g pore volume), higher surface area (192 m<sup>2</sup>/g), and higher saturation magnetization value (14.74 emu/g). The adsorption kinetics and isotherms on all magnetic biochar samples are better fitted to the pseudo-second order and the Sips model rather than Langmuir and Freundlich model which demonstrate a strong adsorption process with high removal efficiency (up to 95%) in a notably fast process where the equilibrium is reached after about 100 minutes. However, the results of adsorption performance obtained from the comparison with commercialized adsorbents indicate that the magnetic biochar in this work still needs and still be able to improve. The advantages of this work are concluded as a simple method that can be able to convert waste to economic materials, as well as contribute greatly to the decrease and control of wild and natural species such as water hyacinth.

#### Data Availability

All the data were concluded in the submission. A supplementary file is available for more details descriptions and explanations throughout the work.

#### Conflicts of Interest

The authors declare that they have no conflicts of interest.

#### Acknowledgments

This work has been supported by the National Research Foundation of Korea (NRF) grant funded by the Korean government (MSIT) (NRF-2019R1C1C1007907 and NRF-2017M3A9E2065287). The author would also express gratitude toward Van Lang University (VLU) for its excellent support for research funding (VLU Research Funding

2022) and the experimental facility. All experiments were carried out in the School of Engineering and Technology (VLSET) laboratory, Van Lang University (VLU). Sogang University (South Korea) supported analytical processes on each sample.

#### Supplementary Materials

Supplementary Materials Additional data and information in this work have been concluded and stated in the supplementary file. The supplementary files include: (i) Table S1 concludes the physicochemical properties of the dried water hyacinth used in this work as input material. (ii) Table S2 provides characteristics of the influent used in this work. (iii) Table S3 concludes with comparison references for the adsorption performance of Pb(II) with different applied adsorbents. (iv) Figure S1 provides more information about the pyrolysis chamber. (v) Figure S2 provides EDS results on the prepared samples which indicate the successful impregnates of cobalt content on the sludge samples. (*Supplementary Materials*)

#### References

- [1] N. A. A. Qasem, R. H. Mohammed, and D. U. Lawal, "Removal of heavy metal ions from wastewater: a comprehensive and critical review," *Npj Clean Water*, vol. 36, no. 4, 2021.
- [2] A. Kaushal and S. Sk, "Adsorption phenomenon and its application in removal of lead from wastewater: a review," *International Journal of Hydrology*, vol. 1, no. 2, pp. 38–47, 2017.
- [3] I. Salihi, S. R. M. Kutty, and M. H. Isa, "Adsorption of lead ions onto activated carbon derived from sugarcane bagasse," *IOP Conference Series: Materials Science and Engineering*, vol. 201, article 012034, 2017.
- [4] M. Manyangadze, N. M. H. Chikuruwo, T. B. Narsaiah et al., "Adsorption of lead ions from wastewater using nano-silica spheres synthesized on calcium carbonate templates," *Heliyon*, vol. 6, no. 11, article e05309, 2020.
- [5] V. D. Tobias, J. L. Conrad, B. Mahardja, and S. Khanna, "Impacts of water hyacinth treatment on water quality in a tidal estuarine environment," *Biological Invasions*, vol. 21, no. 12, pp. 3479–3490, 2019.
- [6] E. Honlah, A. Y. Segbefia, D. O. Appiah, M. Mensah, and P. O. Atakora, "Effects of water hyacinth invasion on the health of the communities, and the education of children along with River Tano and Abby-Tano Lagoon in Ghana, Cogent," *Social Sciences*, vol. 5, no. 1, 2019.
- [7] S. H. Ho, Y. D. Chen, Z. K. Yang, D. Nagarajan, J. S. Chang, and N. Q. Ren, "High-efficiency removal of lead from wastewater by biochar derived from anaerobic digestion sludge," *Bioresource Technology*, vol. 246, pp. 142–149, 2017.
- [8] K. Kaetzl, M. Lubken, T. Gehring, and M. Wichern, "Efficient low-cost anaerobic treatment of wastewater using biochar and woodchip filters," *Water*, vol. 10, no. 7, p. 818, 2018.
- [9] Z. Feng, R. Yuan, F. Wang, Z. Chen, B. Zhou, and H. Chen, "Preparation of magnetic biochar and its application in catalytic degradation of organic pollutants: a review," *Science of The Total Environment*, vol. 765, p. 142673, 2021.
- [10] Z. Ajmal, A. Muhmood, R. Dong, and S. Wu, "Probing the efficiency of magnetically modified biomass-derived biochar for effective phosphate removal," *Journal of Environmental Management*, vol. 253, p. 109730, 2020.

- [11] D. Chen, X. Wang, X. Zhang, Y. Yang, Y. Xu, and G. Qian, "Facile fabrication of mesoporous biochar/ZnFe<sub>2</sub>O<sub>4</sub> composite with enhanced visible-light photocatalytic hydrogen evolution," *International Journal of Hydrogen Energy*, vol. 44, no. 36, pp. 19967–19977, 2019.
- [12] R. Chatterjee, B. Sajjadi, W. Y. Chen et al., "Effect of pyrolysis temperature on physicochemical properties and acoustic-based amination of biochar for efficient CO<sub>2</sub> adsorption," *Frontiers in Energy Research*, vol. 8, no. 8, p. 2020, 2020.
- [13] P. R. Yaashikaa, P. S. Kumar, S. Varjani, and A. Saravanan, "A critical review on the biochar production techniques, characterization, stability and applications for circular bioeconomy," *Biotechnology Reports*, vol. 28, p. e00570, 2020.
- [14] W. Cai, J. Wei, Z. Li, Y. Liu, J. Zhou, and B. Han, "Preparation of amino-functionalized magnetic biochar with excellent adsorption performance for Cr(VI) by a mild one-step hydrothermal method from peanut hull," *Colloids and Surfaces A: Physicochemical and Engineering Aspects*, vol. 563, pp. 102–111, 2019.
- [15] Z. Niu, W. Feng, H. Huang et al., "Green synthesis of a novel Mn-Zn ferrite/biochar composite from waste batteries and pine sawdust for Pb<sup>2+</sup> removal," *Chemosphere*, vol. 252, p. 126529, 2020.
- [16] J. Alchouron, C. Navarathna, H. D. Chludil et al., "Assessing South American Guadua chacoensis bamboo biochar and Fe<sub>3</sub>O<sub>4</sub> nanoparticle dispersed analogs for aqueous arsenic(V) remediation," *Science of The Total Environment*, vol. 706, p. 135943, 2020.
- [17] F. Allam, M. Elnouby, K. M. El-Khatib, D. E. El-Badan, and S. A. Sabry, "Water hyacinth (*Eichhornia crassipes*) biochar as an alternative cathode electrocatalyst in an air-cathode single chamber microbial fuel cell," *International Journal of Hydrogen Energy*, vol. 45, no. 10, pp. 5911–5927, 2020.
- [18] X. Liu, R. Yi, N. Zhang, R. Shi, X. Li, and G. Qiu, "Cobalt hydroxide nanosheets and their thermal decomposition to cobalt oxide nanorings," *Chemistry-An Asian Journal*, vol. 3, no. 4, pp. 732–738, 2008.
- [19] Z. Liu, R. Ma, M. Osada, K. Takada, and T. Sasaki, "Selective and controlled synthesis of  $\alpha$ - and  $\beta$ -cobalt hydroxides in highly developed hexagonal platelets," *American Chemical Society*, vol. 127, no. 40, pp. 13869–13874, 2005.
- [20] T. K. Tran, N. Kim, H. J. Leu, M. P. Pham, N. A. Luong, and H. K. Vo, "The production of hydrogen gas from modified water hyacinth (*Eichhornia crassipes*) biomass through a pyrolysis process," *International Journal of Hydrogen Energy*, vol. 46, no. 27, pp. 13976–13984, 2021.
- [21] S. N. F. Moridon, M. N. I. Salehmin, K. Arifin, L. J. Minggu, and M. B. Kassim, "Synthesis of cobalt oxide on FTO by hydrothermal method for photoelectrochemical water splitting application," *Applied sciences*, vol. 11, no. 7, p. 3031, 2021.
- [22] Y. C. Liu, J. A. Koza, and J. A. Switzer, "Conversion of electrodeposited Co(OH)<sub>2</sub> to CoOOH and Co<sub>3</sub>O<sub>4</sub> and comparison of their catalytic activity for the oxygen evolution reaction," *Electrochimica Acta*, vol. 140, pp. 359–365, 2014.
- [23] P. Wang, M. Cao, C. Wang, Y. Ao, J. Hun, and J. Qian, "Kinetics and thermodynamics of adsorption of methylene blue by a magnetic graphene-carbon nanotube composite," *Applied Surface Science*, vol. 290, pp. 116–124, 2014.
- [24] I. L. Rodriguez, M. Calero, G. Blazquez, and M. A. M. Lara, "Greenhouse crop residue and its derived biochar: potential as adsorbent of cobalt from aqueous solutions," *Water*, vol. 12, no. 5, p. 1282, 2020.
- [25] Y. Tu, Z. Peng, P. Xu et al., "Characterization and application of magnetic biochars from corn stalk by pyrolysis and hydrothermal treatment," *BioResources*, vol. 12, no. 1, pp. 1077–1089, 2016.
- [26] N. Hossain, S. Nizamuddin, G. Griffin, R. Selvakannan, N. M. Mubarak, and T. M. I. Mahlia, "Synthesis and characterization of rice husk biochar via hydrothermal carbonization for wastewater treatment and biofuel production," *Scientific Reports*, vol. 10, no. 1, p. 18851, 2020.
- [27] Y. Liu, G. Zhu, B. Ge, H. Zhou, A. Yuan, and X. Shen, "Concave Co<sub>3</sub>O<sub>4</sub> octahedral mesocrystal: polymer-mediated synthesis and sensing properties," *CrystEngComm*, vol. 14, no. 19, pp. 6264–6270, 2012.
- [28] T. He, D. Chen, X. Jiao, Y. Xu, and Y. Gu, "Surfactant-assisted solvothermal, synthesis of Co<sub>3</sub>O<sub>4</sub> hollow spheres with oriented-aggregation nanostructures and tunable particle size," *Langmuir*, vol. 20, no. 19, pp. 8404–8408, 2004.
- [29] X. Jian, S. Li, Y. Feng et al., "Influence of synthesis methods on the high-efficiency removal of Cr(VI) from aqueous solution by Fe-modified magnetic biochars," *ACS Omega*, vol. 5, no. 48, pp. 31234–31243, 2020.
- [30] P. Zhang, S. J. Dong, H. H. Ma, B. X. Zhang, Y. F. Wang, and X. M. Hu, "Fractionation of corn stover into cellulose, hemicellulose, and lignin using a series of ionic liquids," *Industrial Crops and Products*, vol. 76, pp. 688–696, 2015.
- [31] R. Khandanlou, G. C. Ngoh, and W. T. Chong, "Feasibility study and structural analysis of cellulose isolated from rice husk: microwave irradiation, optimization, and treatment process scheme," *Bioresources*, vol. 11, no. 3, pp. 5751–5766, 2016.
- [32] S. Vijayakumar, A. K. Ponnalagi, S. Nagamuthu, and G. Muralidharan, "Microwave assisted synthesis of Co<sub>3</sub>O<sub>4</sub> nanoparticles for high-performance supercapacitors," *Electrochimica Acta*, vol. 106, pp. 500–505, 2013.
- [33] R. K. Gupta, A. K. Sinha, B. N. R. Sekhar, A. K. Srivastava, G. Singh, and S. K. Deb, "Synthesis and characterization of various phases of cobalt oxide nanoparticles using inorganic precursor," *Applied Physics A*, vol. 103, no. 1, pp. 13–19, 2011.
- [34] M. T. Yang, Y. Du, W. C. Tong, A. C. K. Yip, and K. Y. A. Lin, "Cobalt-impregnated biochar produced from CO<sub>2</sub>-mediated pyrolysis of Co/Lignin as an enhanced catalyst for activating peroxymonosulfate to degrade acetaminophen," *Chemosphere*, vol. 226, pp. 924–933, 2019.
- [35] R. Tian, H. Dong, J. Chen, R. Li, and Q. Xie, "Amorphous Co<sub>3</sub>O<sub>4</sub> nanoparticles-decorated biochar as an efficient activator of peroxymonosulfate for the removal of sulfamethazine in aqueous solution," *Separation and Purification Technology*, vol. 250, p. 117246, 2020.
- [36] L. Kemmou, Z. Frontistis, J. Vakros, L. D. Manariotis, and D. Mantzavinos, "Degradation of antibiotic sulfamethoxazole by biochar-activated persulfate: factors affecting the activation and degradation processes," *Catalysis Today*, vol. 313, pp. 128–133, 2018.
- [37] E. B. C. Santos, C. G. Moreno, J. J. P. Barros et al., "Effect of alkaline and hot water treatment on the structure and morphology of piassava fibers," *Materials Research*, vol. 21, no. 2, 2018.
- [38] G. Bali, X. Meng, J. I. Deneff, Q. Sun, and A. J. Ragauskas, "The effect of alkaline pretreatment methods on cellulose structure and accessibility," *ChemSusChem*, vol. 8, no. 2, pp. 275–279, 2014.
- [39] N. Sumrith, L. Techawinyutham, M. R. Sanjay, R. Dangtungee, and S. Siengchin, "Characterization of alkaline and silane

- treated fiber of 'water hyacinth plants' and reinforcement of 'water hyacinth fiber' with bioepoxy to develop fully biobased sustainable eco-friendly composites," *Journal of Polymer and the Environment*, vol. 28, no. 10, pp. 2749–2760, 2020.
- [40] S. Rezania, H. Alizadeh, J. Cho et al., "Changes in composition and structure of water hyacinth based on various pretreatment methods," *BioResources*, vol. 14, no. 3, pp. 6088–6099, 2019.
- [41] C. Liu, L. Chen, D. Ding, and T. Cai, "From rice straw to magnetically recoverable nitrogen-doped biochar: efficient activation of peroxymonosulfate for the degradation of metolachlor," *Applied Catalysis B: Environmental*, vol. 254, pp. 312–320, 2019.
- [42] B. Wang, Y. Li, J. Zheng, Y. Hu, X. Wang, and B. Hu, "Efficient removal of U (VI) from aqueous solutions using the magnetic biochar derived from the biomass of a bloom-forming cyanobacterium (*Microcystis aeruginosa*)," *Chemosphere*, vol. 254, p. 126898, 2020.
- [43] D. D. Sewu, H. N. Tran, G. O. Boahen, and S. H. Woo, "Facile magnetic biochar production route with new goethite nanoparticle precursor," *Science of the Total Environment*, vol. 717, p. 137091, 2020.
- [44] Y. Tu, Y. Xiong, C. Descorme, L. Kong, and S. Tian, "Heterogeneous photo-Fenton oxidation of acid orange II over iron-sewage sludge derived carbon under visible irradiation," *Journal of Chemical Technology and Biotechnology*, vol. 89, no. 4, pp. 544–551, 2014.
- [45] O. Xin, H. Yitong, C. Xi, and C. Jiawei, "Magnetic biochar combining adsorption and separation recycle for removal of chromium in aqueous solution," *Water Science and Technology*, vol. 75, no. 5, pp. 1177–1184, 2017.
- [46] Y. Han, X. Cao, X. Ouyang, S. P. Sohi, and J. Chen, "Adsorption kinetics of magnetic biochar derived from peanut hull on the removal of Cr (VI) from aqueous solution: effects of production conditions and particle size," *Chemosphere*, vol. 145, pp. 336–341, 2016.
- [47] B. Chen, Z. Chen, and S. Lv, "A novel magnetic biochar efficiently sorbs organic pollutants and phosphate," *Bioresource Technology*, vol. 102, no. 2, pp. 716–723, 2011.
- [48] W. Zhang and I. M. Lo, "EDTA-enhanced washing for remediation of Pb- and/or Zn-contaminated soils," *Journal of Environmental Engineering*, vol. 132, no. 10, pp. 1282–1288, 2006.
- [49] Y. Hu, Y. Zhu, Y. Zhang et al., "An efficient adsorbent: simultaneous activated and magnetic ZnO doped biochar derived from camphor leaves for ciprofloxacin adsorption," *Bioresource Technology*, vol. 288, p. 121511, 2019.
- [50] D. Cheng, H. H. Ngo, W. Guo et al., "Feasibility study on a new pomelo peel derived biochar for tetracycline antibiotics removal in swine wastewater," *Science of The Total Environment*, vol. 720, p. 137662, 2020.
- [51] B. Peng, L. Chen, C. Que et al., "Adsorption of antibiotics on graphene and biochar in aqueous solutions induced by  $\pi$ - $\pi$  interactions," *Scientific Reports*, vol. 6, pp. 1–10, 2016.
- [52] Y. Wang, X. Xiao, and B. Chen, "Biochar impacts on soil silicon dissolution kinetics and their interaction mechanisms," *Scientific Reports*, vol. 8, p. 8040, 2018.
- [53] Y. Wang, X. Xiao, Y. Xu, and B. Chen, "Environmental effects of silicon within biochar (sichar) and carbon-silicon coupling mechanisms: a critical review," *Environmental Science & Technology*, vol. 53, no. 23, pp. 13570–13582, 2019.
- [54] T. Chen, Z. Zhou, R. Han, R. Meng, H. Wang, and W. Lu, "Adsorption of cadmium by biochar derived from municipal sewage sludge: impact factors and adsorption mechanism," *Chemosphere*, vol. 134, pp. 286–293, 2015.
- [55] E. Mehrvarz, M. Jahanshahi, and A. A. Ghoreyshi, "Adsorptive separation of CO<sub>2</sub> and CH<sub>4</sub> by the broom sorghum-based activated carbon functionalized by diethanolamine," *ResearchGate*, vol. 34, no. 2, pp. 413–424, 2017.
- [56] M. Belhachemi and F. Addoun, "Comparative adsorption isotherms and modeling of methylene blue onto activated carbons, applied water," *Science*, vol. 1, pp. 111–117, 2011.
- [57] J. Ifthikar, J. Wang, Q. Wang et al., "Highly efficient lead distribution by magnetic sewage sludge biochar: sorption mechanisms and bench applications," *Bioresource Technology*, vol. 238, pp. 399–406, 2017.
- [58] D. Mohan, P. Singh, A. Sarswat, P. H. Steele, and C. U. Pittman Jr., "Lead sorptive removal using magnetic and nonmagnetic fast pyrolysis energy cane biochars," *Journal of Colloid and Interface Science*, vol. 448, pp. 238–250, 2015.
- [59] J. C. M. Posada, S. Salas, and I. V. Abunader, "Factors affecting relative abundance of low-mobility fishing resources: spiny lobster in the Galapagos marine reserve," *Creative Commons Attribution License*, vol. 7, 2019.
- [60] A. A. Alghamdi, A. B. A. Odayni, W. S. Saeed, A. A. Kahtani, F. A. Alharthi, and T. Aouak, "Efficient adsorption of lead (II) from aqueous phase solutions using polypyrrole-based activated carbon," *Material*, vol. 12, no. 12, p. 2020, 2019.
- [61] W. Wu, J. Li, T. Lan et al., "Unraveling sorption of lead in aqueous solutions by chemically modified biochar derived from coconut fiber: a microscopic and spectroscopic investigation," *Science of the Total Environment*, vol. 576, pp. 766–774, 2017.
- [62] D. H. K. Reddy and S. M. Lee, "Magnetic biochar composite: facile synthesis, characterization, and application for heavy metal removal," *Colloids, and Surface A: Physicochemical and Engineering Aspects*, vol. 454, pp. 96–103, 2014.